Engineering Fracture Mechanics 229 (2020) 106949

Contents lists available at ScienceDirect

Engineering Fracture Mechanics

journal homepage: www.elsevier.com/locate/engfracmech

Identification of fracture toughness parameters to understand the fracture resistance of advanced high strength sheet steels

D. Frómeta[a,*], S. Parareda[a], A. Lara[a], S. Molas[a], D. Casellas[a,b], P. Jonsén[b], J. Calvo[c]

[a] Eurecat, Centre Tecnològic de Catalunya, Unit of Metallic and Ceramic Materials, Plaça de la Ciència, 2, Manresa 08243, Spain
[b] Division of Mechanics of Solid Materials, Luleå University of Technology, 971 87 Luleå, Sweden
[c] Universitat Politècnica de Catalunya, Eduard Maristany 16, 08019 Barcelona, Spain

ARTICLE INFO

Keywords:
Fracture toughness
J-integral
Essential work of fracture
Kahn tear tests
Advanced high strength steel sheets

ABSTRACT

The fracture toughness of four advanced high strength steel (AHSS) thin sheets is evaluated through different characterization methodologies, with the aim of identifying the most relevant toughness parameters to describe their fracture resistance. The investigated steels are: a Complex Phase steel, a Dual Phase steel, a Trip-Aided Bainitic Ferritic steel and a Quenching and Partitioning steel. Their crack initiation and propagation resistance is assessed by means of *J-integral* measurements, essential work of fracture tests and Kahn-type tear tests. The results obtained from the different methodologies are compared and discussed, and the influence of different parameters such as specimen geometry or notch radius is investigated. Crack initiation resistance parameters are shown to be independent of the specimen geometry and the testing method. However, significant differences are found in the crack propagation resistance values. The results show that, when there is a significant energetic contribution from necking during crack propagation, the specific essential work of fracture (w_e) better describes the overall fracture resistance of thin AHSS sheets than J_C. In contrast, energy values obtained from tear tests overestimate the crack propagation resistance and provide a poor estimation of AHSS fracture performance. w_e is concluded to be the most suitable parameter to describe the global fracture behaviour of AHSS sheets and it is presented as a key property for new material design and optimization.

1. Introduction

A vast array of new multiphase advanced high strength steels (AHSS) has been developed in the last two decades in order to fulfil the automotive industry's demands on lightweighting and passive safety. These steels represent one of the best cost-effective, lightweight solutions for auto body and chassis components. Therefore, considerable research efforts are being devoted to the development of optimized microstructures for enhanced structural integrity and impact performance. One of the key steps in material optimization is the establishment of appropriate characterization techniques to understand the role of microstructural constituents on fracture behaviour and predict in-service performance. Nevertheless, with the emergence of AHSS, this task has become even more challenging.

The limited ductility of AHSS compared to conventional mild steels has raised new cracking-related issues that cannot be rationalized via traditional uniaxial tensile testing approaches and classical ductility rankings based on elongation values. For example,

* Corresponding author.
E-mail address: david.frometa@eurecat.org (D. Frómeta).

https://doi.org/10.1016/j.engfracmech.2020.106949
Received 10 December 2019; Received in revised form 10 February 2020; Accepted 21 February 2020
Available online 02 March 2020

Nomenclature

a	crack length
A_{50}	elongation at fracture (initial gauge length 50 mm)
A_g	uniform elongation
A_{pl}	plastic area under load-displacement curve
β	plastic zone shape factor
δ_5	crack opening displacement measured over an initial gauge length of 5 mm
E	Young's modulus
ε_{ij}	strain tensor
ε_u	true uniform strain
ε_f	true fracture strain
Γ	integration path of the contour integral
J	*J*-integral
J_i	*J*-integral at crack initiation
J_c	*J*-integral near the onset of stable crack propagation
K	stress intensity factor
K_{IC}	mode I plane strain fracture toughness
l_o	initial ligament length
n	strain hardening exponent
P	applied load
R curve	crack growth resistance curve
ρ	notch root radius
σ_{ij}	stress tensor
σ_{YS}	yield stress
σ_{UTS}	ultimate tensile strength
σ_f	fracture stress
t_o	initial thickness
t_f	specimen thickness after fracture
Ti	traction vector components
u_p	actual plastic displacement
w	strain energy density
W	specimen width
W_f	total work of fracture
W_e	essential work of fracture
W_p	non-essential plastic work
w_f	total specific work of fracture
w_f^i	specific work of fracture initiation
w_e	specific essential work of fracture
w_e^i	specific essential work of fracture initiation
w_p	non-essential specific plastic work

Abbreviations

AHSS	advanced high strength steel
CP	complex phase steel
CT	compact tension specimen
CTOA	crack tip opening angle
CTOD	crack tip opening displacement
DENT	double edge notched tension specimen
DP	dual phase steel
EDM	electrical discharge machining
EPFM	elastic plastic fracture mechanics
EWF	essential work of fracture
FPZ	fracture process zone
HER	hole expansion ratio
PHS	press hardened steel
Q&P	quenching and partitioning steel
SENT	single edge notched tension specimen
TE	total elongation
TRIP	transformation induced plasticity steel
TWIP	twinning induced plasticity steel
UIE	unit initiation energy
UPE	unit propagation energy
UTS	ultimate tensile strength

it has been recurrently evidenced in the literature that steels with greater elongation (both uniform and total) can be more susceptible to the appearance of fractures in trimmed, sheared or punched areas during cold forming (edge cracking, hole expansion, stretch flanging) [1–6]. Similar behaviour has been observed in the crash failure behaviour of AHSS and press hardened steels (PHS). It has been shown that steels with higher ductility can exhibit poorer crash ability and a higher amount of cracking during impact loading [7–11]. In this context, fracture toughness, measured in the frame of fracture mechanics, has shown to be the most adequate property to understand this kind of fractures related to the material's crack initiation and propagation resistance [3–6,11].

The contributions of Yoon et al. [3] and Casellas et al. [4] showed a strong correlation between fracture toughness and the edge cracking resistance of multiple AHSS sheets, evaluated in terms of hole expansion ratio (HER). This approach has been further discussed in [5] and [6], where the edge formability of different complex phase (CP) and dual phase (DP) steels is investigated and related to their crack propagation resistance. More recent works have also shown that fracture mechanics can be effectively used to classify and understand the impact performance, as well as other fractures related to the local ductility of AHSS and PHS [11,12]. Therefore, fracture toughness has become a relevant property for new high strength sheet material development and optimization.

However, over the years, little attention has been paid to the cracking resistance of such high strength metal sheets for automotive applications and, thus, limited information is available in the literature. The main reason lies in the intrinsic complexity of elastic plastic fracture mechanics (EPFM) methodologies and the historical absence of standard methods to characterize the fracture toughness of thin ductile sheets under plane stress conditions.

The ASTM E1820 [13] describes the standard procedure for evaluating the fracture toughness of metallic materials by means of the traditional *J-integral* and *Crack Tip Opening Displacement* (*CTOD*) measurements. However, it is intended for plane strain fracture toughness characterization and the defined specimen thickness requirements are not satisfied for thin sheets. Alternative standards were developed later for the evaluation of resistance to stable crack extension of thin-gauge materials, the ASTM E2472 [14] and the ISO 22889 [15]. These standards propose the use of alternative parameters for fracture resistance characterization, the *Crack Tip Opening Angle* (*CTOA*) and the crack opening displacement δ_5, expressed in terms of a resistance curve, δ_5-*R*. However, as pointed out before, such standard EPFM methodologies are experimentally very complex. They require expert technical skill for specimen preparation and the crack advance must be monitored during the whole test, which represents one of the main challenges in fracture mechanics testing procedures. Additionally, they usually involve complex data processing and, such as in the case of the *CTOA*

fracture criterion, the use of finite element method analysis, which makes the application of the methods expensive and time-consuming. Thus, alternative simpler and faster experimental approaches have been developed in order to satisfy the growing need for knowing the fracture properties of thin metallic sheets.

Owing to its experimental simplicity, the essential work of fracture (EWF) method [16] has become one of the most attractive alternatives to assess the ductile tearing resistance of thin metallic sheets [16–27] and polymers [28–31]. Recently, many authors have also used the EWF methodology to characterize the cracking resistance of several AHSS and PHS sheets [4–6,11,12,32–38]. The main advantage of this method is that it is very easy to perform and avoids the need for measurement of the crack extension.

Another testing technique to readily evaluate the fracture resistance of thin metal sheets that has received considerable interest is the Kahn-type tear test [39]. This simple energy-based method offers a valuable tool for indexing the tearing resistance of ductile metal sheets and evaluating the effect of the processing parameters and the microstructural constituents on overall toughness. It has been applied to characterize the toughness of precipitation hardening aluminium alloys [39–42], AHSS [7,12], PHS [43] and twinning-induced plasticity (TWIP) steels [44].

Some researchers have also proposed alternative non-standard single specimen methods based on *J-integral* measurements. For instance, Faccoli et al. [45] used the *J-integral* expressions proposed by Rice et al. [46] for double edge notched tension (DENT) specimens to evaluate the fracture resistance of a TWIP steel, a DP steel and two Quenching and Partitioning (Q&P) steels. A similar approach was used by Luo et al. [37] and Xiong et al. [47,48] to investigate the fracture behavior of different TWIP [37] and Q&P [47,48] microstructures.

According to the number of recent publications dealing with this topic, it is evident that research interest in the fracture behavior of thin AHSS sheets has increased significantly in the last years. However, there are still some uncertainties regarding the effect of different testing variables (specimen geometry, notch radius, etc.) on fracture toughness measurements or which are the most suitable parameters to define the fracture resistance of these sheet materials.

Within this framework, the main aim of the present paper is to briefly review and discuss some of the different existing experimental approaches to evaluating the fracture toughness of thin ductile sheets and to investigate the relevance of the measured toughness parameters to describe the fracture resistance of AHSS sheets. Moreover, it is also aimed at providing a better understanding of the influence of different experimental variables on the obtained toughness values. For this purpose, the fracture toughness of four AHSS sheets typically used in automotive industry is investigated using different EPFM-based characterization techniques. The materials investigated are: a CP, a DP, a Transformation Induced Plasticity (TRIP)-aided Bainitic Ferritic (TBF) and a Q&P steel. Fracture toughness is evaluated through *J-integral* measurements, EWF tests and Kahn-type tear tests. Comparison is made between the different crack initiation and propagation resistance parameters obtained, and their main similarities and differences are discussed. The influence of the notch root radius and the specimen geometry on the measured toughness values is also assessed.

2. Materials

The materials investigated in this work are two conventional first generation AHSS (CP and DP) and two third generation TRIP-aided AHSS grades (TBF and Q&P). The steels were supplied in the form of sheets of 1.4–1.5 mm. The chemical composition of the steels is shown in Table 1. Engineering and true tensile stress-strain curves and mechanical properties for the transverse direction are shown in Fig. 1 and Table 2 respectively. True stress-strain curves are represented up to the uniform strain (ε_u) and extrapolated to the fracture strain (ε_f). The microstructures of the investigated AHSS grades were characterized by means of Scanning Electron Microscopy (SEM). The resulting SEM micrographs are shown in Fig. 2.

The microstructure of the CP steel consists of a homogeneous bainite/tempered martensite matrix (Fig. 2a). These steels are characterized by high yield stress to tensile strength ratio and low strain hardening. They have a great energy absorption capacity and good local formability (hole expansion, bending on tight radius, etc.), which makes them especially suitable for crash resistant parts [11,12]. DP microstructure presents a combination of ferrite/bainitic ferrite and martensite (Fig. 2b). Such mixture of soft (ferrite) and hard (martensite) phases results in great strain hardening and high elongation values. Usually, DP steels exhibit lower yield stress than CP at equal tensile strengths. They show very good global formability but poorer local ductility and fracture toughness than CP steels [11,12]. TBF steel presents a dual-phase like microstructure, basically consisting of ferrite and bainite, with significant amounts (11%) of metastable retained austenite (Fig. 2c). The replacement of the soft single-phase matrix present in first generation TRIP steels by the harder ferrite/bainite matrix allows attainment of higher strengths, while the good ductility and formability is maintained thanks to the TRIP effect. TBF steels generally exhibit greater strain hardening and larger elongation values (both uniform and total) than DP steels, which results in improved global formability. However, they show limited local formability and axial impact energy absorption [11,12]. The Q&P steel (Fig. 2d) has a homogeneous martensite/bainite matrix with retained austenite (6%). The

Table 1
Chemical composition of the investigated steels (in weight per cent).

Steel grade	C	Si	Mn	Cr	B	Al
CP	0.11	0.34	~2.3	0.12	0.0017	0.040
DP	0.19	0.18	~2.3	0.46	0.0003	0.048
TBF	0.20	0.84	> 2.4	0.17	0.0003	0.039
Q&P	0.12	0.81	> 2.4	0.18	0.0002	0.043

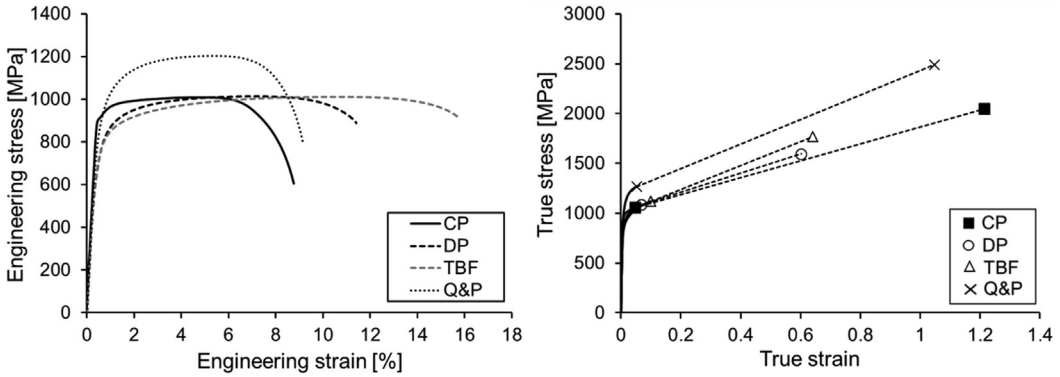

Fig. 1. Engineering and true stress-strain curves. The symbols correspond to the true uniform strain and the true fracture strain.

Table 2
Mechanical properties of the investigated AHSS sheets in transverse direction. t = thickness; σ_{ys} = yield strength; σ_{UTS} = ultimate tensile strength; A_g = uniform elongation (elongation at *UTS*); A_{50} = elongation at fracture (initial gauge length 50 mm); $n_{2\text{-}4}$ = strain hardening exponent between 2 and 4% of deformation; ε_u = true uniform strain; ε_f = true fracture strain; σ_f = fracture stress.

Steel	t [mm]	σ_{ys} [MPa]	σ_{UTS} [MPa]	A_g [%]	A_{50} [%]	$n_{2\text{-}4}$ [–]	ε_u [–]	ε_f [–]	σ_f [MPa]
CP	1.40	915	1008	4.8	8.8	0.05	0.05	1.21	2048
DP	1.40	775	1015	7.0	11.4	0.10	0.07	0.60	1595
TBF	1.50	755	1012	10.5	15.8	0.11	0.10	0.64	1768
Q&P	1.40	920	1202	5.3	9.1	0.10	0.05	1.05	2490

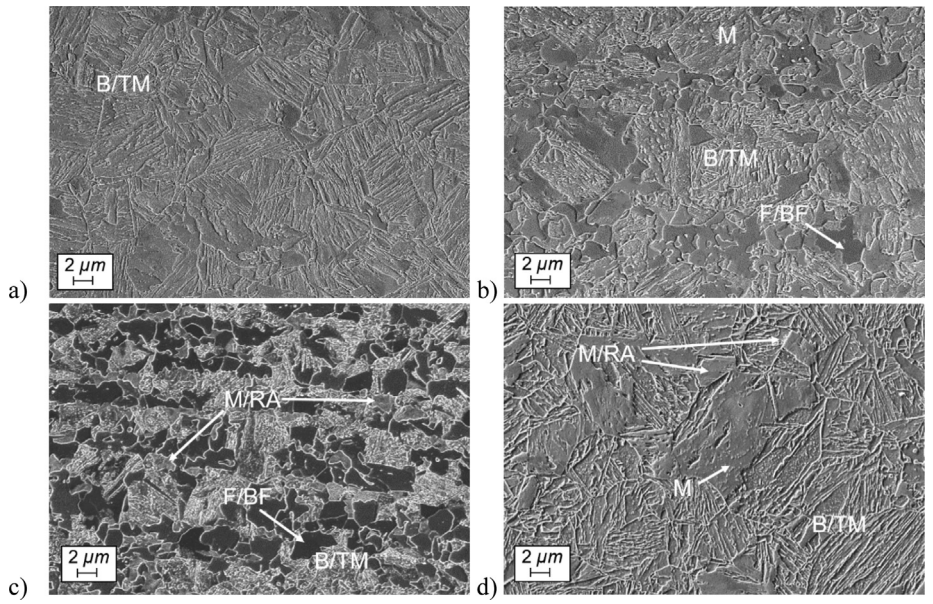

Fig. 2. Microstructures of (a) CP (b) DP (c) TBF and (d) Q&P.

TRIP effect contributes to increased strain hardening, and the presence of hard martensite, rather than bainitic ferrite, leads to higher strength levels than TBF steels, but lower elongation. Q&P steels represent a good option for anti-intrusion structural parts, due to their enhanced bendability and fracture resistance [11,12].

3. Fracture toughness evaluation methods

This section describes the fracture toughness characterization methods used in this work. It is important to note that fracture resistance of thin sheets under plane stress conditions has an extra energetic contribution from necking and, thus, fracture toughness depends on the sheet thickness. Accordingly, all the evaluated fracture toughness parameters shown in the present work are only

representative for the investigated sheet thickness.

3.1. J-integral

The *J-integral* concept was introduced by Rice [49] to characterize the crack tip strain fields in nonlinear elastic materials. The nonlinear energy release rate J can be written as a path independent contour integral:

$$J = \int_{\Gamma} \left(w dx_2 - T_i \frac{\partial u_i}{\partial x_1} ds \right) \tag{1}$$

where Γ is an arbitrary contraclockwise path around the crack tip, w is the strain energy density, T_i are the components of the traction vector, defined according to the outward normal along Γ ($T_i = \sigma_{ij} n_j$), u is the displacement vector and ds is an element of arc length along Γ. The strain energy density w is defined according to Eq. (2):

$$w = \int_0^{\varepsilon_{ij}} \sigma_{ij} d\varepsilon_{ij} \tag{2}$$

where σ_{ij} and ϵ_{ij} are the stress and strain tensors, respectively.

Since the first works of Begley and Landes [50,51] and Rice et al. [46], the *J*-integral has been the most widely used fracture parameter to characterize the fracture toughness of elastic-plastic materials. It is evaluated in terms of a critical *J*-integral value (*Jc*) for stationary cracks and *J-Resistance* (*J-R*) curves for growing cracks.

The method for the evaluation of J_c and the construction of *J-Resistance (J-R)* curves is described in the standard ASTM E1820 [13]. However, as mentioned above, this standard was developed to evaluate the fracture toughness of metallic materials under plane strain conditions. Thus, specimen size requirements are not fulfilled by many thin sheet materials, as those investigated in this work. For example, considering a thickness of 1.5 mm and the proportions given in the standard for a Compact Tension (CT) specimen ($2 \leq W/B \leq 4$, where W is the distance between the load line and the back end of the specimen and B is the sheet thickness), a specimen with a maximum size of 7.2 × 7.5 mm could be used, which would severely hamper its manipulation and testing.

Nevertheless, Zhu and Leis [52] showed that, if the thickness requirement is not considered, it is possible to apply the ASTM E1820 to evaluate a *J-R* curve in thin sheet ductile materials. To avoid such size constraints, in this study CT specimens for *J-integral* measurements were machined following the recommendations of the ASTM E561 [53]. The ASTM E561 was developed for measuring the *K–R* curve of thin gauge materials and is therefore less restrictive concerning the specimen size. The geometry of the CT specimen used is shown in Fig. 3a. All the specimens were machined with the crack oriented along the rolling direction (T-L). The initial notch was prepared by electrical discharging machining (EDM). A fatigue pre-crack was nucleated from the starting notch and extended 5 mm, resulting in an initial crack size (notch + fatigue pre-crack) of 18 mm ($a/W = 0.64$). For each material, a *J-R* curve was constructed according to ASTM E1820 (Fig. 3b). The crack advance was measured by means of a high resolution video camera located in one of the sides of the specimen (frame rate: 30 images/s). The fracture tests were performed in a universal testing machine under displacement control at a constant cross-head speed of 1 mm/min and the load vs load-line displacement curves were recorded. The load-line displacement was measured by means of a clip-on displacement gage.

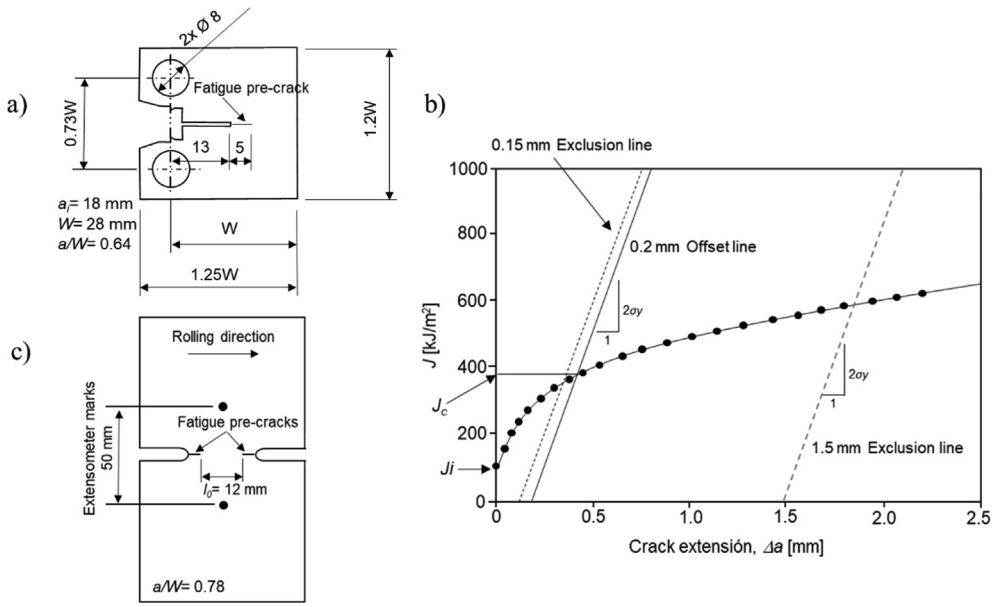

Fig. 3. (a) CT specimen geometry used for *J-integral* measurements. (b) Construction of the J-R curve according to ASTM E1820 and determination of the fracture toughness parameters J_i and J_c. (c) DENT specimen for *J-integral* measurements.

From the *J-R* curves, two cracking resistance parameters were obtained: the fracture toughness at cracking initiation, J_i, which is the toughness value at the point at which first crack extension is detected in the video equipment (subcritical crack initiation), and the fracture toughness near the onset of stable crack propagation, J_c, obtained from the intersection of the 0.2 mm offset line with the *R* curve as indicated in ASTM E 1820.

Additionally, in order to evaluate the effect of the specimen geometry on J_i and J_c determination, *J-integral* measurements were performed with DENT specimens. For the evaluation of J_i, the equation proposed by Rice et al. [46] for a DENT specimen was used:

$$J = \frac{K^2}{E} + \frac{1}{t_0 l_0}\left(2\int P du_p - P u_p\right) \tag{3}$$

where K is the stress intensity factor, which for a DENT specimen is given by Eq. (4) [54]:

$$K = \frac{P\sqrt{\pi a}}{t_0 \cdot 2W\sqrt{1-\frac{a}{W}}}\left[1.122 - 0.561\left(\frac{a}{W}\right) - 0.205\left(\frac{a}{W}\right)^2 + 0.471\left(\frac{a}{W}\right)^3 - 0.190\left(\frac{a}{W}\right)^4\right] \tag{4}$$

E is the elastic modulus, t_0 is the specimen thickness, l_0 is the uncracked ligament length, P is the actual load and u_p is the actual plastic displacement. In Eq. (4), W refers to the half of the specimen width. Eq. (3) is only applicable to stationary cracks. Thus, to account for the crack growth incremental equations must be used as indicated in [55]:

$$J_n = J_{n-1} + \frac{2(A_{pl(n)} - A_{pl(n-1)})}{t_0(l_{n-1} + l_n)} + \frac{2(K_n^2 l_n - K_{n-1}^2 l_{n-1})}{E(l_{n-1} + l_n)} \tag{5}$$

where *n* and *n-1* denote two consecutive points on the recorded load vs load-line displacement curve, A_{pl} refers to the plastic area under the curve and l is the actual ligament length. The parameters E, K and t_0 are defined above.

The geometry of the DENT specimens used for *J-integral* measurements is shown in Fig. 3c. Notches were prepared by EDM and extended by fatigue pre-cracks ($\approx$1.5 mm per side). The initial ligament length (l_0) was of 12 mm (a/W = 0.78). The displacement was measured by means of a videoextensometer using two extensometer marks on the specimen separated 50 mm. The rest of the testing conditions were the same as described above for the CT specimens.

3.2. Essential work of fracture

The idea of the essential work of fracture (EWF) was initially proposed by Broberg [56,57]. He suggested that the ductile fracture process takes place in two different regions: an inner fracture process zone (FPZ) and an outer plastic region. Later, Cotterel and Reddel developed a methodology to experimentally separate these two terms, the EWF methodology [16]. The work developed in the FPZ is called the essential work of fracture (W_e). It represents the energy necessary to create new surfaces at the front of the crack tip and it is proportional to the fractured area. The work dissipated in the outer plastic zone is the non-essential plastic work (W_p), which depends on the volume of the deformed region around the fracture plane. Then, the total work of ductile fracture can be expressed as follows:

$$W_f = W_e + W_p = w_e l_0 t_0 + \beta w_p l_0^2 t_0 \tag{6}$$

where w_e is the specific essential work of fracture per unit area, l_0 is the ligament length, t_0 is the specimen thickness, w_p is the specific non-essential plastic work per unit volume and β is a shape factor that depends on the shape of the plastic zone. Normalizing Eq. (6) by the cross-section area gives:

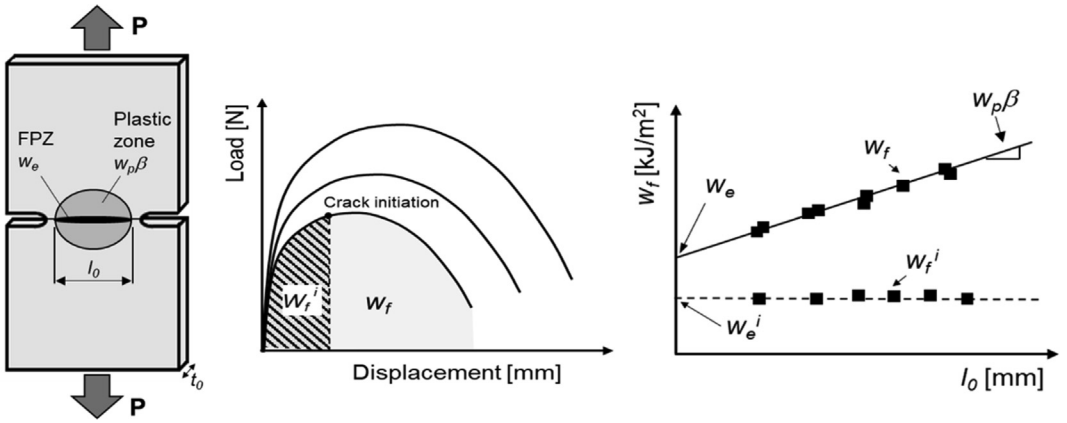

Fig. 4. DENT specimen and experimental procedure for the determination of the essential work of fracture, w_e and the specific work for fracture initiation, w_e^i.

$$\frac{W_f}{l_0 t_0} = w_f = w_e + \beta w_p l_0 \tag{7}$$

Thus, if a series of w_f values are plotted against the ligament length (l_0), w_e and βw_p can be obtained by linear regression, where w_e is given by the intercept and βw_p by the slope, as shown in Fig. 4. w_f values are obtained by integrating the area under load vs displacement curves (W_f) and dividing by $l_0 t_0$. By definition, w_e measures the energy dissipated within the FPZ and, thus, it is a suitable parameter to describe the crack propagation resistance of thin ductile sheets. Many authors have addressed the equivalence between w_e and *J-integral* [21,22,28–30]. Such equivalence is further discussed in Section 4.

The EWF methodology also allows separation of energetic contributions from crack initiation and crack propagation and determination of a crack initiation toughness value, the specific essential work for fracture initiation, w_e^i [29]. The specific work for fracture initiation, w_f^i is calculated by integrating the area under load vs displacement curve until the onset of crack propagation. As shown by Mai and Cotterel [29], w_f^i is independent of the ligament length. Therefore, w_e^i is calculated from an average of w_f^i values from different ligament lengths (Fig. 4).

In this work, w_e and w_e^i have been obtained by testing rectangular DENT specimens of 240 × 55 mm. The specimen geometry and the loading conditions were the same as for *J-integral* measurements (Fig. 3c, Section 3.1). Ligament lengths (l_0) ranging from 5 to 15 mm (a/W: 0.73 ÷ 0.9) were used. Crack initiation was detected by means of a high resolution video camera synchronized with the testing machine. In order to evaluate the effect of the notch radius on the EWF, two different notch conditions were evaluated: notch machined by EDM (ρ ≈ 150 μm) and EDM notch + fatigue pre-crack (ρ ≈ 0.1 μm).

Results for fatigue pre-cracked specimens are extracted from reference [11]. *wf* vs l_0 plots have been included and w_e^i has been recalculated with additional specimens.

3.3. Kahn-type tear tests

The Kahn-type tear tests were originally developed by Kaufman and Knoll [39] to characterize the notch resistance of thin aluminium sheets. The tear test consists in loading up to fracture a single edge notched tensile (SENT) specimen with a very sharp notch at a constant displacement rate and recording the load and displacements required to fracture the specimen (the characteristic load vs load-line displacement curve of the tear test is shown in Fig. 5). Then, the notch resistance is characterized by the *UIE* (Unit Initiation Energy) and the *UPE* (Unit Propagation Energy).

UIE represents the energy necessary (both elastic and plastic) to nucleate a crack and is obtained by integration of the area under the load vs load-line displacement curve up to the displacement corresponding to the maximum load (Fig. 5). *UPE* is the energy per unit area necessary to propagate a crack in a tear specimen up to fracture. *UPE* is the primary result of the tear test and it is obtained by integrating the area of the load vs load-line displacement curve from the point of maximum load to the displacement at fracture (Fig. 5). It represents a measure of the combination of ductility and strength of the material and it can be used as a relative index of toughness. It cannot be considered as an absolute measure of the material's crack propagation resistance since it is geometry dependent. However, the good correlation observed between *UPE* and plane strain fracture toughness, K_{Ic} [39,58], shows that *UPE* can be a suitable parameter for ranking the tearing resistance of thin ductile alloys.

The standard procedure for the tear testing of aluminium alloys products is described in ASTM B871 [59]. Even though the method was developed for aluminium alloys, many authors have shown the suitability of the Kahn-type tear tests to characterize the tearing resistance of AHSS [7,12,43,44]. For example, Ying et al. [43] used the Kahn-type tear tests to investigate the effect of different processing parameters (austenization temperature, soaking time and start deformation temperature) on the strength and toughness of PHS sheets. Lorthios et al. [44] also used these tear tests to study the damage mechanisms of a high Mn TWIP steel.

In the present work, Kahn type tear tests were performed according to ASTM B871 [59]. The notch was prepared by EDM (ρ ≈ 150 μm). All the specimens were machined with the notch oriented along the rolling direction (T-L specimens). The tests were conducted at a constant speed of 1 mm/min. Due to the compression load in the final stage of fracture, the specimens never fractured

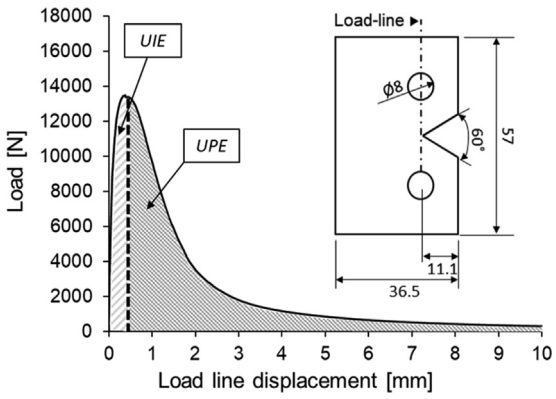

Fig. 5. Load vs load-line displacement curve from Kahn-type tear tests and specimen geometry used for the tear tests.

completely. Therefore, the tests were manually stopped at 10 mm of displacement when load is steadily decreased to zero. For load-line displacement measurement, initial extensometer marks separated 10 mm were placed in the specimen. 3 specimens per material and condition were tested. The high resolution video camera was used to check that crack initiation coincided with the point of maximum load.

4. Results and discussion

4.1. J-integral measurements

Fig. 6 shows the J-R curves obtained for the investigated AHSS grades. J_i and J_c values are given in Table 3. At a first glance, two types of fracture behaviour can be distinguished. On the one hand, CP and Q&P show the highest *J integral* values, both at cracking initiation ($J_{i\ CT}$ = 125 kJ/m^2 and 118 kJ/m^2 respectively) and near the onset of stable crack propagation ($J_{c\ CT}$ = 248 kJ/m^2 and 260 kJ/m^2 for CP and Q&P respectively). Both steel grades exhibit very similar *J-R* curves, characterized by a pronounced slope in the initial part of the curve (blunting line) and a noteworthy increase of *J* values during crack propagation. On the other hand, DP and TBF show substantially lower J_i and J_c values and flatter resistance curves, which indicate that energetic contribution to crack propagation resistance is significantly reduced in these two steels compared to CP and Q&P steels. In this case, DP and TBF have similar *J integral* values at crack initiation ($J_{i\ CT}$ = 84 kJ/m^2 for DP and $J_{i\ CT}$ = 89 kJ/m^2 for TBF) and at the onset of stable crack propagation ($J_{c\ CT}$ = 144 kJ/m^2 and 169 kJ/m^2 for DP and TBF respectively). However, TBF presents a *J-R* curve with a slightly steeper slope, which leads to greater *J* values for relatively large crack extensions.

Specimen geometry is shown to have an important influence on the *J-R* curve, but not on J_i and J_c values. As observed in Fig. 6, the resistance curves obtained with CT and DENT specimens converge in the initial part of the plot, providing similar values of J_i and J_c for all the investigated materials. However, as the crack grows, DENT specimens show higher *J* values than CT specimens, describing a steeper *R* curve. These results are in concordance with the observations of Xia et al. [60] and Zhu et al. [61]. They investigated the effect of the constraint level on *J-R* curve of ductile crack growth by using different specimen geometries. They found that *J-integral* values along the resistance curve decrease with increasing crack tip constraint, whereas little effect of specimen geometry was observed on initiation toughness. They also showed that CT specimens have higher crack tip constraint, and thus lower *J-R* curve, than DENT specimens.

4.2. Essential work of fracture

Fig. 7 and Table 4 show the EWF results obtained for the two investigated notch conditions. The first noticeable thing is the large

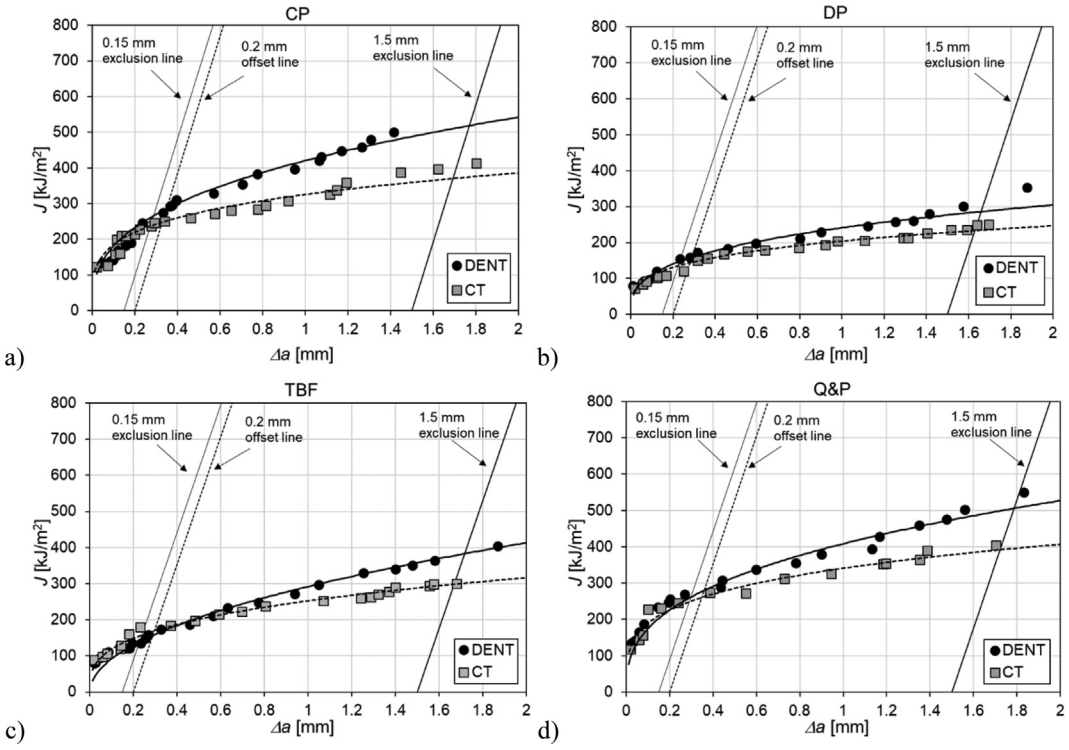

Fig. 6. *J-R* curves for the investigated AHSS grades: (a) CP, (b) DP, (c) TBF and (d) Q&P.

Table 3
Results of *J-integral* measurements with CT and DENT specimens.

	CT		*DENT*	
Steel grade	$J_{i\ CT}$ [kJ/m^2]	$J_{c\ CT}$ [kJ/m^2]	$J_{i\ DENT}$ [kJ/m^2]	$J_{c\ DENT}$ [kJ/m^2]
CP	125	248	135	286
DP	84	144	84	158
TBF	89	169	81	157
Q&P	118	260	135	280

influence of notch root radius on EWF measurements. Values of w_e and w_e^i obtained with notched specimens are much higher than those obtained with fatigue pre-cracked specimens. This effect is particularly relevant for initiation toughness values ($w_e^{i}{}_{crack}/w_{enotch}^{i} = 0.36$ for CP and TBF and 0.39 for DP and Q&P). w_e also shows a strong notch radius dependency, especially in DP, TBF and Q&P ($w_{e\ crack}/w_{e\ notch} = 0.47$, 0.48 and 0.42 respectively). These results indicate that fracture toughness values obtained with notched specimens overestimate the material's fracture resistance and, thus, may lead to misleading conclusions. This is clearly evidenced when comparing CP (Fig. 7a) and Q&P (Fig. 7d). Both steels exhibit very similar fracture behaviour for notched specimens (almost identical w_e, w_e^i and βw_p). Nevertheless, w_e results for fatigue pre-cracked specimens show that Q&P has significantly lower crack propagation resistance than CP.

The influence of notch root radius on fracture toughness measurements is well known in fracture mechanics testing and it has been addressed by several authors [34,35,45,62–64]. All these works showed a linear increase in fracture toughness with the notch radius, ρ. Such *apparent* increase in fracture toughness is related to the decrease in stress triaxility degree with increasing notch root radius and the additional plastic deformation developed at the notch tip, necessary for crack nucleation. However, it has been found that below a critical radius (ρ_c), fracture toughness becomes independent of ρ. The value of ρ_c depends on the material. Akourri et al. [63] found a ρ_c of ≈0.85 mm for a mild steel, Chaudhari et al. [64] obtained a ρ_c of ≈0.15 mm for extra deep drawing steel sheets. A similar value was observed by Faccoli et al. [45] for a TWIP steel. Muñoz et al. [34] showed that a sharp notch of ρ = 0.01 mm (sharpened by razor blade) provided toughness values close to those obtained with fatigue pre-cracks for a DP780.

As observed, some materials are quite insensitive to notch radius, whereas others show high notch radius sensitivity. Therefore, in general, the determination of fracture toughness for a determined notch radius may not be suitable enough to assess the fracture resistance of the material. For this reason, in order to obtain a more realistic notch-independent toughness value, standard fracture toughness testing procedures recommend the use of fatigue pre-cracked specimens [13–15].

In line with the above comments, only w_e and w_e^i values obtained from fatigue pre-cracked specimens are considered to represent the *real* fracture toughness of the investigated steel sheets in the present study. These will be used from this point forward to discuss their crack initiation and propagation resistance.

The results indicate that CP steel has, by far, the highest crack propagation resistance of the analysed steels ($w_{e\ crack} = 405 \pm 11$ kJ/m^2). Q&P shows significantly lower w_e ($w_{e\ crack} = 194 \pm 12$ kJ/m^2), closer to that of DP and TBF ($w_{e\ crack} = 138 \pm 20$ kJ/m^2 and 149 ± 13 kJ/m^2, respectively). Even though DP and TBF steels have very similar w_e values, they show quite different fracture behaviour. As observed in Fig. 7c, TBF shows greater w_f values (comparable to CP and Q&P) than DP for large ligament lengths. However, these values rapidly decrease for smaller ligament lengths, resulting in low w_e and very high βw_p. In Q&P, similarly to the observed in TBF, there is also a large contribution from the plastic work. On the other hand, CP shows significantly lower βw_p, which indicates that most of the energetic contribution to the ductile fracture process comes from the essential work of fracture developed in the FPZ.

The values of w_e^i also reveal that CP and Q&P have greater crack initiation resistance than DP and TBF. Nonetheless, in this case the differences between the different steels are not as significant as observed for w_e values. Q&P shows the highest w_e^i ($w_e^{i}{}_{crack} = 172 \pm 2$ kJ/m^2), closely followed by CP ($w_e^{i}{}_{crack} = 156 \pm 14$ kJ/m^2). DP and TBF show the lowest toughness at crack initiation ($w_e^{i}{}_{crack} = 110 \pm 12$ kJ/m^2 and 110 ± 16 kJ/m^2, respectively).

It is worth mentioning that, for pre-cracked specimens, crack initiation was detected before the maximum load in all the investigated steels. Accordingly, the (often used) peak load criterion for fracture initiation may result in inappropriate initiation toughness values and, therefore, it must be experimentally assessed for every material.

4.3. Kahn-type tear tests

Fig. 8a shows the load vs load-line displacement curves obtained from the Kahn-type tear tests. *UIE* and *UPE* values are shown in Fig. 8b and Table 5. In this case, the assumption that crack initiation coincided with the point of maximum load was confirmed for all the studied materials. As observed, CP and Q&P show superior *UIE* to DP and TBF. It is interesting to note that, even though Q&P reaches higher load than CP during the tear test (Pmax ≈ 17.1 kN and 14.9 kN respectively), both steels show similar *UIE*. This can be explained by the greater displacement at maximum load shown by CP (dPmax = 0.46 mm for CP and 0.40 mm for Q&P). As illustrated in Fig. 8a, TBF reaches similar P_{max} (≈14.8 kN) to CP but at significantly smaller displacement ($d_{Pmax} = 0.34$ mm), which results in poorer *UIE*. DP exhibits the lowest *UIE* of the investigated steels. It shows similar displacement at maximum load to TBF ($d_{Pmax} = 0.33$ mm) and the lowest P_{max} (≈13.6 kN). Looking at *UPE* values, it can be seen that CP has the greatest propagation energy, followed by TBF and Q&P. Finally, DP has the poorest crack propagation resistance.

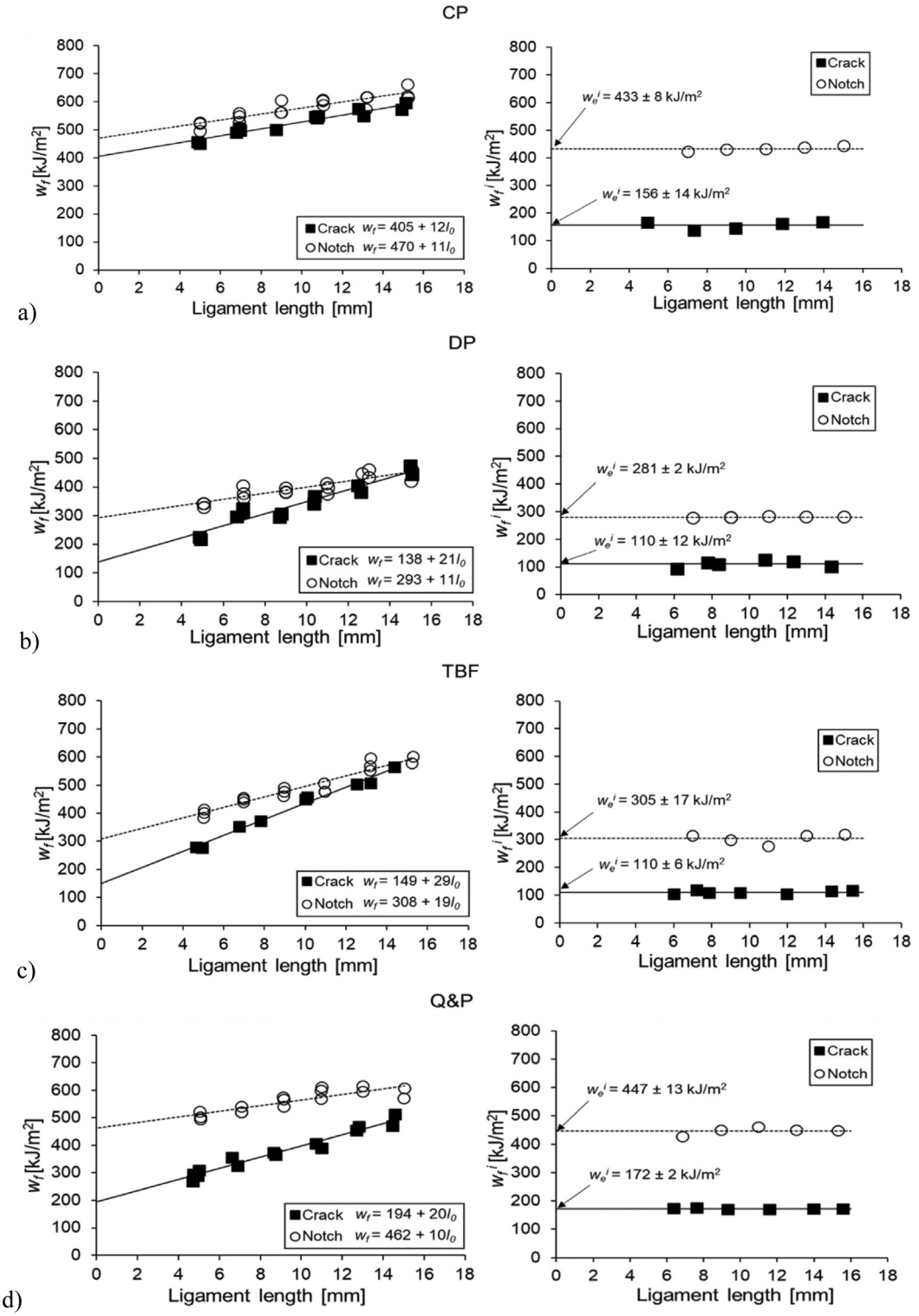

Fig. 7. EWF results for the investigated AHSS grades: (a) CP, (b) DP, (c) TBF and (d) Q&P. Solid symbols correspond to the EWF values obtained with fatigue pre-cracked specimens, open symbols correspond to notched specimens. Left: w_f values as a function of the ligament length. Right: w_f^i values as a function of the ligament length. The average cracking initiation value (w_e^i) is indicated.

The different tearing behavior of the steels can be discerned from their load vs displacement curves. DP, TBF and Q&P show a sudden load drop just after crack initiation (P_{max}) and the load rapidly decreases with increasing displacement. This effect is

Table 4
EWF results. Results for fatigue pre-cracked specimens are extracted from reference [11]. The values of $w_e{}^i{}_{crack}$ can be slightly different, since they have been recalculated.

	Crack (ρ = 0.1 μm)			Notch (ρ = 150 μm)		
Steel grade	$w_e{}^i{}_{crack}$ [kJ/m^2]	$w_{e\ crack}$ [kJ/m^2]	$\beta w_{p\ crack}$ [MJ/m^3]	$w_e{}^i{}_{notch}$ [kJ/m^2]	$w_{e\ notch}$ [kJ/m^2]	$\beta w_{p\ notch}$ [MJ/m^3]
CP	156 ± 14	405 ± 11	12 ± 1	433 ± 8	470 ± 14	11 ± 1
DP	110 ± 12	138 ± 20	21 ± 2	281 ± 2	293 ± 15	11 ± 1
TBF	110 ± 16	149 ± 13	29 ± 1	305 ± 17	308 ± 15	19 ± 1
Q&P	172 ± 2	194 ± 12	20 ± 1	447 ± 13	462 ± 16	10 ± 2

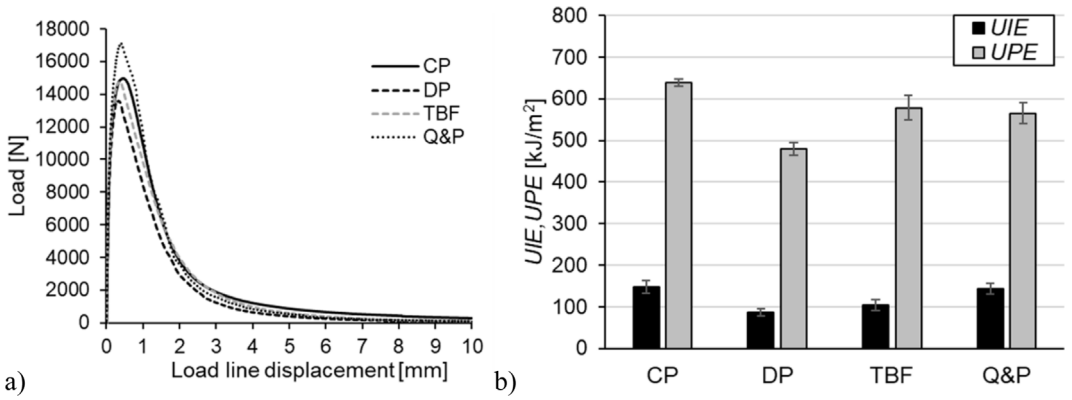

Fig. 8. (a) Load vs load-line displacement curves from Kahn-type tear tests. Only one representative curve per material is plotted. (b) *UIE* and *UPE* for the investigated AHSS.

Table 5
Results of Kahn-type tear tests.

Steel grade	*UIE* [kJ/m^2]	*UPE* [kJ/m^2]
CP	147 ± 15	639 ± 10
DP	87 ± 9	479 ± 15
TBF	104 ± 12	579 ± 30
Q&P	144 ± 13	566 ± 26

especially relevant in Q&P, which shows slightly lower *UPE* than TBF, and DP. CP, in turn, shows a more gradual decrease in the load after P_{max}, which justifies the higher energetic contribution to crack propagation resistance.

4.4. Comparison of fracture toughness parameters

This section is intended to summarize the obtained fracture resistance values according to the different methodologies and to discuss their main differences and similarities.

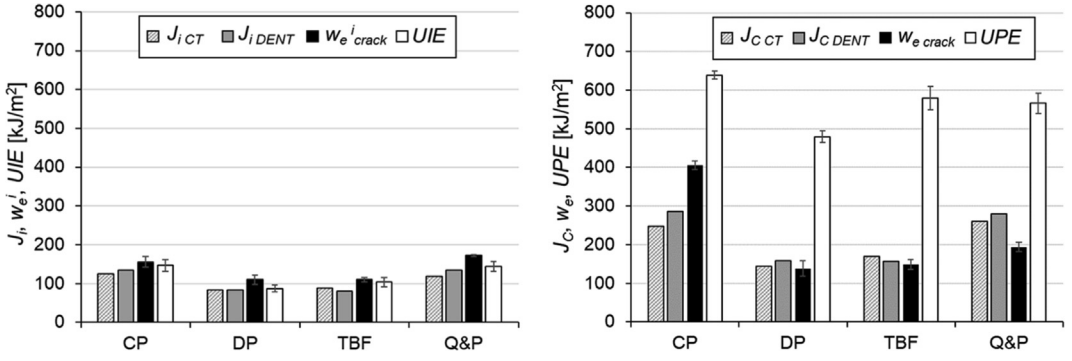

Fig. 9. Summary of crack initiation (left) and crack propagation resistance (right) parameters. Standard deviation is indicated when available.

Fig. 9 shows the different crack initiation and propagation resistance parameters evaluated in this work. The results of EWF measurements with notched specimens are not considered for discussion. It is important to note that J_c, by definition, is not strictly speaking a crack propagation resistance value but it represents the fracture toughness for a small amount of crack extension. Nevertheless, it is plotted together with the crack propagation resistance parameters, w_e and *UPE* to differentiate it from the initiation toughness J_i. This differentiation is important and will be the basis for discussing the relation between J_c and w_e in the following paragraphs.

As shown in Fig. 9 left, crack initiation resistance values are independent of the specimen geometry and the testing methodology used. Surprisingly, in spite of the larger notch radius used in Kahn type specimens, initiation toughness results of tear tests are very similar to those obtained from *J-integral* and EWF measurements with fatigue pre-cracked specimens. It is assumed then, that for this specimen configuration, the stress concentration ahead of the notch tip closely resembles that of a crack and, therefore, a machined sharp notch ($\rho = 150$ μm) is suitable enough to obtain representative toughness values. This contrasts highly with the significant influence of notch root radius observed in DENT specimens for EWF measurements and represents an advantage with respect to the other methods, since the need for time-consuming fatigue pre-cracking procedures is avoided.

However, while *UIE* provides a good estimation of fracture toughness at crack initiation, *UPE* completely overestimates the crack propagation resistance of the material. Fig. 9 right shows that *UPE* is much higher than w_e for all the investigated AHSS grades. Such large discrepancy between *UPE* and w_e can be explained by means of the energy partitioning concept described in Section 3.2, which states that the ductile fracture process has two main energetic contributions: one from the plastic work surrounding the crack plane and other developed in the FPZ, necessary to create new surfaces in the front of the crack tip. In Kahn type tear tests, both contributions are intermingled, i.e. *UPE* contains not only the energy for new surfaces creation but also that of the plastic work. The plastic work is geometry dependent and, therefore, cannot be considered a material property. For this reason, the results from the tear tests must be taken with care and only as a relative index of toughness.

On the other hand, w_e only quantifies the energy dissipated in the FPZ, since the contribution from the plastic work is mathematically removed by extrapolation to ligament zero. As demonstrated by several authors [28,29,66], w_e is an intrinsic material property (for a given sheet thickness) independent of specimen geometry. The relation between w_e and J_c has been repeatedly discussed in literature [21,22,28–30,65]. Wu and Mai [28] and Mai and Cotterell [29] found a very good agreement between w_e and the critical *J-integral* value for different ductile polymers. Mai and Cotterell [65] also differentiated between J_i and J_c (they called it J_p) and showed that w_e^i and w_e were equivalent to J_i and J_c respectively. The correspondence between J_i and w_e^i is corroborated in Fig. 9 left. However, important differences are observed between w_e and J_c. DP and TBF show similar values of w_e ($w_e = 138 \pm 20$ and 149 ± 13 kJ/m^2, respectively) and J_c ($J_{c\ CT} = 144$ and 169 kJ/m^2 respectively). By contrast, in CP and Q&P, w_e ($w_e = 405 \pm 11$ and 194 ± 12 kJ/m^2) significantly differs from J_c ($J_{c\ CT} = 248$ and 260 kJ/m^2, respectively).

Again, it must be kept in mind that J_c and w_e are conceptually different, since J_c is a toughness value for a small crack advance (given by the ASTM E1820) and w_e is an average crack propagation resistance value for the complete fracture process. Furthermore, as shown by Cotterell and Atkins [66], *J-integral* includes, besides the contribution from the essential work of fracture, the plastic work dissipated out of the FPZ. Pardoen et al. [22] suggested that, when there is small contribution from crack propagation after

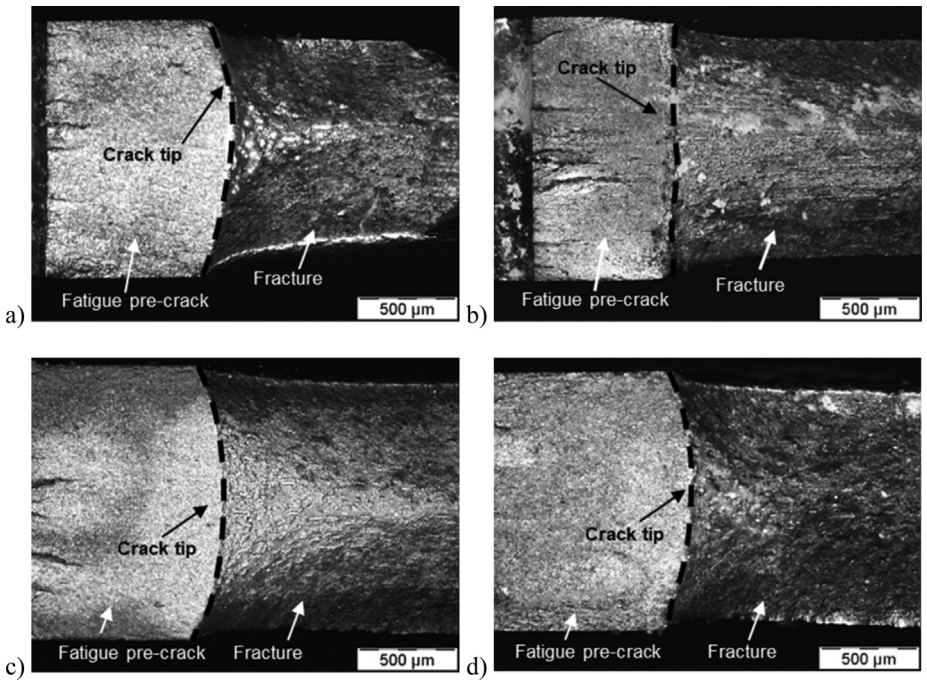

Fig. 10. Fracture surface of DENT specimens: (a) CP (b) DP (c) TBF (d) Q&P.

initiation ($w_e \approx w_e^i$), J_c can be equivalent to w_e. Nevertheless, when there is significant contribution from crack propagation ($w_e \gg w_e^i$), w_e and J_c are different. In plane stress ductile fracture, such contribution to crack propagation resistance developed in the FPZ comes primarily from necking. The evolution of necking during fracture for the studied steel grades is analysed in Figs. 10 and 11. Fig. 10 shows the fracture surface of DENT specimens used for *J-integral* and EWF measurements. In Fig. 11, the true thickness strain (ε_3) is plotted as a function of the distance from the crack tip. True thickness strain is calculated according to Eq. (8):

$$\varepsilon_3 = ln\left(\frac{t_0}{t_f}\right) \tag{8}$$

where t_0 is the initial thickness and t_f is the thickness after fracture. It can be seen that steels with lower w_e^i (DP and TBF) show a lower degree of necking at the crack tip. The differences between w_e and w_e^i can be also explained by the progress of the thickness strain along the FPZ. DP, TBF and Q&P steels, which have $w_e \approx w_e^i$, show small increase of true thickness strain, which is rapidly stabilized at approximately 0.3 mm from the crack tip ($\varepsilon_{3\,ss}/\varepsilon_{3\,tip} \approx 1.7$, 1.5 and 1.2 for DP, TBF and Q&P respectively. $\varepsilon_{3\,ss}$ is the true thickness strain for the steady state and $\varepsilon_{3\,tip}$ is the true thickness strain at crack tip). On the other hand, in CP ($w_e \gg w_e^i$) the degree of necking progressively increases to reach a steady value of $\varepsilon_3 = 0.26$ at approximately 0.5 mm from crack tip ($\varepsilon_{3\,ss}/\varepsilon_{3\,tip} \approx 2.2$).

Such contribution from necking to the ductile fracture process supposes a real increment in the crack propagation resistance of the material [22] and it is effectively measured by w_e. In contrast, in *J-integral* measurements this contribution can be masked due to the additional energy from plastic work. This explains why CP and Q&P have practically identical *J-R* curves (Fig. 6). They show similar energy values for the same crack advance. However, as shown in Section 4.2, this energy comes from different contributions: In CP, it derives from the essential work of fracture dissipated in the FPZ (which justifies the large differences between w_e and J_c) whereas in Q&P, it comes from the non-essential plastic work.

The fact that Q&P shows greater J_c than w_e may be related to the additional energy associated to the 0.2 mm of crack advance. Looking at the resistance curve, it is observed that the transition in the initial slope occurs for a crack advance of approximately 0.1 mm. At this point, J values are in the range of 200–220 kJ/m^2, which are in better agreement with w_e. According to these observations, it can be asserted that when the fracture process has an important contribution from the crack propagation, w_e better represents the tearing resistance of thin ductile sheets than J_c.

4.5. Relation between fracture toughness and tensile strength/fracture properties

Several attempts have been made to correlate fracture properties and uniaxial tensile strength-elongation parameters. For instance, the product of the ultimate tensile strength (*UTS*) by the total elongation (*TE*) has been often used in literature as a toughness indicator. This parameter represents a combination of the material's strength and ductility and it is conventionally used as a performance index of AHSS [67]. The true fracture strain (ε_f) derived from the reduction of area at fracture in tensile tests is also used as a measure of the material's fracture resistance and it has been recently proposed as a relative index of local formability [67]. The common perception is that greater fracture strain or greater $UTS \times TE$ product imply greater fracture toughness. However, as has been proven by different authors [11,32,48], no clear link can be established between fracture toughness of AHSS and these parameters or other related tensile strength/ductility properties. Such assumption is refuted again in Fig. 12. The figure shows no relation between the $UTS \times TE$ product and the different fracture toughness parameters investigated in this study. Furthermore, looking at J_c and w_e, an opposite trend to that expected is observed, i.e. steels with greater $UTS \times TE$ show lower fracture toughness. Similar observations were made by Xiong et al. in various Q&P steels [48]. They also found that the true fracture strain or the product of the fracture stress and the true fracture strain ($\sigma_f \times \varepsilon_f$) were not suitable either to rank toughness. For the steel grades characterized in this study, such tensile fracture parameters seem to provide a better estimation of fracture toughness (Fig. 12), especially in terms of cracking initiation (J_i, w_e^i, *UIE*) and J_c. Nevertheless, they do not capture the large differences in full tearing resistance measured by w_e (Fig. 12b). No clear correlation can be determined either between any of the plotted tensile parameters and *UPE* values from tear tests. Therefore, it is important to highlight again that fracture resistance of high strength sheet materials cannot be estimated from

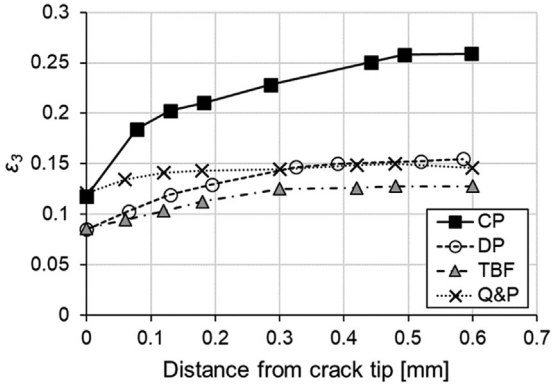

Fig. 11. True thickness strain as a function of the distance from the crack tip.

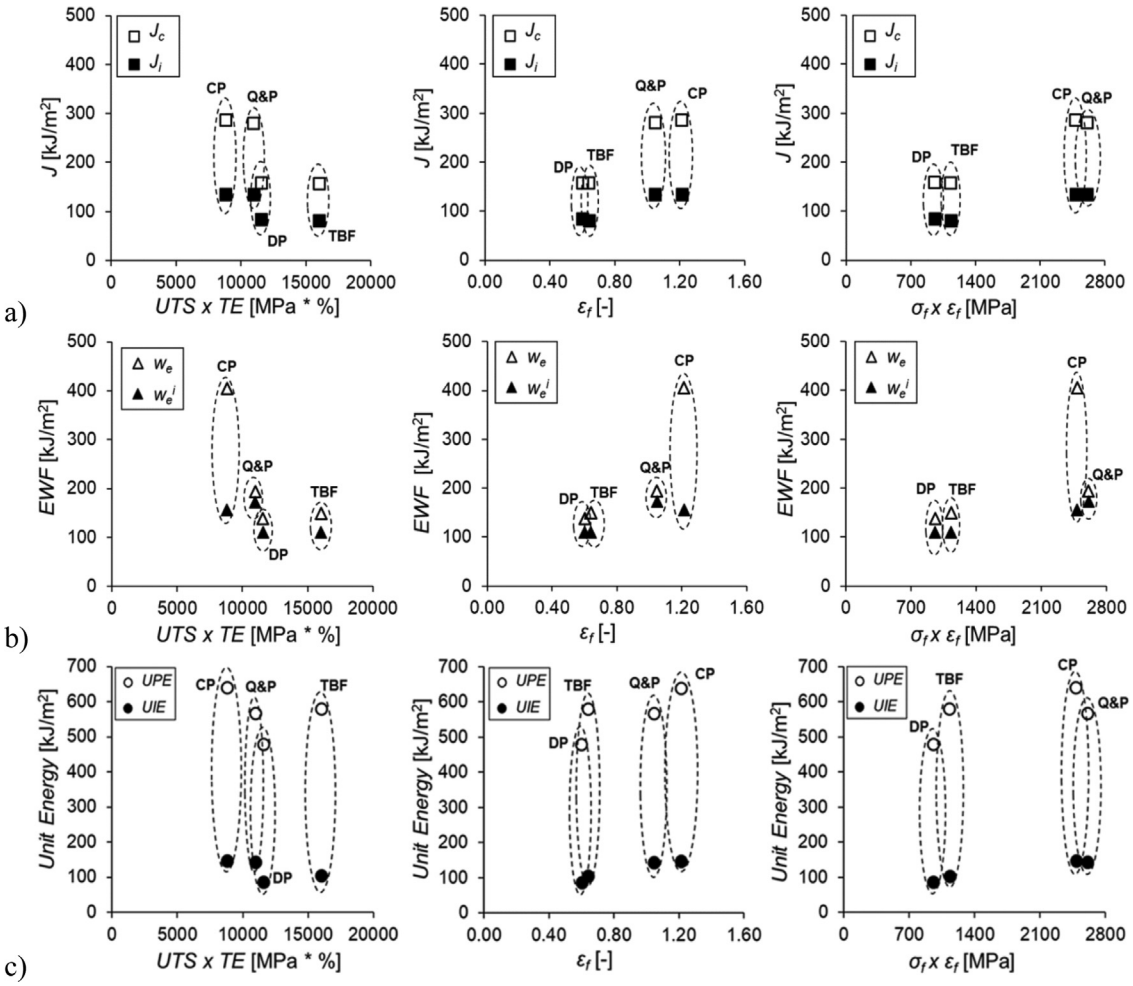

Fig. 12. Fracture toughness as a function of: product of ultimate tensile strength (*UTS*) and total elongation (*TE*); true fracture strain (ε_f); product of fracture stress (σ_f) and true fracture strain (ε_f). (a) J-integral results, (b) EWF results and (c) Kahn-type tear tests results.

tensile properties.

4.6. Application of fracture toughness to understand high strength steel sheet performance

As mentioned before, several research studies have evidenced that fracture toughness is a useful property to rationalize and predict cracking-related phenomena in AHSS sheets, such as edge fractures, crash failure or local formability issues [3–6,11,12]. However, the results obtained in this work show the importance of selecting the adequate toughness parameters to understand the fracture behaviour of these steels and avoid erroneous material rankings. This is illustrated in Fig. 13, where the different crack initiation and propagation resistance values obtained in this work are plotted against edge cracking resistance (in terms of hole expansion ratio), and crashworthiness, expressed as the absorbed energy per unit area in axial impact tests. Published toughness values for AHSS grades of similar thickness and *UTS* are also plotted (data extracted from reference [12]). Detailed information about the experimental procedure for edge cracking and crash resistance characterization is given in [4] and [11] respectively.

As reported in previous works, both edge cracking [4–6] and crash resistance [11,12] of AHSS are strongly related to the specific essential work of fracture, w_e (linear fitting with $R^2 = 0.86$ and 0.95 respectively). In contrast, the investigated crack initiation resistance parameters (J_i, w_e^i, *UIE*) show no clear correlation either with HER or axial impact energy. It indicates that this kind of fractures, as discussed in [11] and [12], is governed by the full tearing resistance of the material rather than by initiation toughness. Therefore, for materials with large contribution from the crack propagation resistance to the complete fracture process, the values of toughness at crack initiation completely underestimate the fracture performance.

CP steel is a clear example of this. As observed in Fig. 13, it shows significantly greater edge cracking resistance and axial impact energy than Q&P (HER = 85 ± 4% and 55 ± 8%; Impact energy per unit area = 36.5 MJ/m^2 and 14.1 MJ/m^2, respectively). Such different fracture behaviour is in good agreement with the differences observed in their overall crack propagation resistance, measured by w_e. Nevertheless, crack initiation resistance is very similar for both steels. Something similar occurs with J_c, which, as

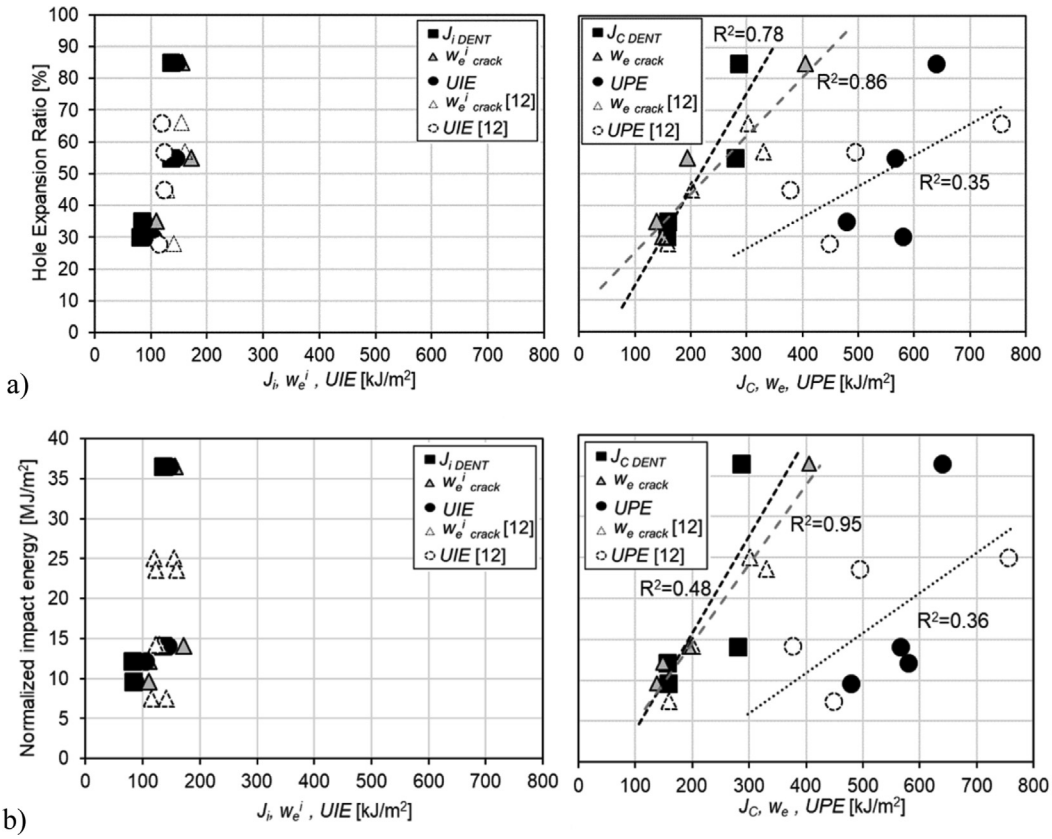

Fig. 13. Correlation between fracture toughness and: (a) edge cracking resistance, expressed as the hole expansion ratio [12]; (b) crashworthiness, in terms of normalized axial impact energy [12]. The fracture toughness parameters investigated in this work (solid symbols) are plotted together other published toughness values (open symbols) [12]. Left: Crack initiation resistance. Right: Crack propagation resistance (correlation coefficient is indicated).

discussed in the previous section, is not suitable enough to describe the full fracture resistance of thin ductile materials with significant crack propagation prior to final failure. *UPE* from tear tests has also been shown to be an unreliable parameter for measuring the crack propagation resistance of thin AHSS sheets. Not only does it overestimate the fracture energy but it can also lead to incorrect toughness estimations, as observed for TBF and Q&P (Fig. 9). This justifies the poor correlation of *UPE* with edge cracking ($R^2 = 0.35$) and axial impact resistance ($R^2 = 0.36$) shown in Fig. 13. The correlation of w_e, *UPE* and local ductility of AHSS sheets is further discussed in [12].

These results indicate that w_e is the most suitable material property to understand the overall fracture performance of thin AHSS sheets. This is a relevant conclusion to take into consideration when using fracture toughness to address the fracture resistance of these steels. Furthermore, it implies w_e as a key property for the development of new AHSS microstructures with enhanced cracking resistance.

5. Conclusions

The fracture toughness of four AHSS sheets for automotive applications has been evaluated through different fracture characterization methodologies and using different specimen geometries and notch conditions. The different tested methodologies, i.e. *J-integral*, EWF and Kahn tear tests, give different values of the energy spent for crack initiation (J_i, w_e^i and *UIE*) and for crack propagation (J_c, w_e and *UPE*). Such differences are discussed below and recommendations for their application to understand the mechanical performance of high strength sheets are given.

Based on the results of the investigations regarding the effect of specimen geometry and notch root radius on fracture toughness measurements, the following conclusions can be drawn:

- The crack initiation resistance (J_i, w_e^i and *UIE*) is independent of the specimen geometry (CT, DENT, Kahn type specimen).
- The specimen geometry has no influence on the determination of the *J-integral* at crack initiation (J_i) and near the onset of stable crack propagation (J_c). However, a significant influence of specimen geometry has been observed in *J* values after a relatively large crack advance. This is attributed to the different crack tip constraint for the investigated geometries.

- Notch root radius has been shown to have a significant influence on EWF measurements. In order to obtain accurate and reliable fracture toughness values, fatigue pre-cracked specimens must be used. Otherwise, the measured toughness values can overestimate the real crack initiation and propagation resistance of the material.

The main differences between the fracture toughness parameters characterized by the three techniques have been discussed and the most relevant conclusions are:

- Kahn type tear tests have been shown to be suitable enough to estimate crack initiation resistance. However, *UPE* values completely overestimate crack propagation resistance, since they include energetic contribution from the plastic work dissipated in the outer zone of the FPZ. Therefore, *UPE* cannot be considered a material property and gives inappropriate toughness ranking.
- Some materials (such as CP steel) may show a large contribution of crack propagation resistance after initiation. In this case, a single crack initiation resistance parameter (J_i, w_e^i or *UIE*) is very conservative and clearly underestimates the overall fracture resistance.
- w_e has been shown to better quantify the crack propagation resistance of thin high strength sheets than J_c. Whereas w_e contains both the energy dissipated during crack initiation and crack propagation to failure, J_c only has energetic contribution from small crack extension and does not account for the complete fracture. *J-R* curves are also unsuitable to represent the *real* crack propagation resistance of the material, because they also include extrinsic contribution from the plastic work dissipated out of the FPZ.
- The additional contribution to the essential work of fracture developed in the FPZ after crack initiation comes mainly from necking. Thus, those materials developing remarkable necking during crack propagation have greater crack propagation resistance.From the analysis of the link between fracture toughness parameters and tensile properties it can be concluded that:
- Conventional toughness estimations based on $UTS \times TE$ product are not suitable to describe the fracture toughness of AHSS. It may lead to wrong material ranking in terms of fracture toughness.
- For the steel grades investigated in this study, tensile fracture parameters, such as the true fracture strain (ε_f) or the product of fracture stress and true fracture strain ($\sigma_f \times \varepsilon_f$), give a better estimation of toughness at cracking initiation and J_c. However, they can underestimate the crack propagation resistance of the material. Therefore, to avoid misleading conclusions about the cracking resistance of high strength sheet metals, fracture toughness must be measured within the framework of fracture mechanics.

Finally, it is concluded that w_e is the most suitable fracture parameter to rationalize crack-related problems in high strength sheets, such as edge fracture or crash behaviour, since they are closely related to the overall energy for the complete fracture rather than to the initiation. Crack initiation parameters, such as w_e^i, *Ji* and *UIE* may underestimate the fracture performance. *UPE* from Kahn type tear tests is not a reliable parameter to predict the kinds of fractures related to the material's crack propagation resistance.

Declaration of Competing Interest

We declare that we have no conflict of interest.

Acknowledgments

The research leading to these results has been partially funded by the EU Horizon 2020 programme under grant agreement H2020-EU.2.1.3. – 814517 (FormPlanet). The authors would like to thank voestalpine Stahl GmbH for supplying the steel sheets. We would also like to acknowledge associate professor Kjell Eriksson at Solid Mechanics, Luleå University of Technology (Sweden), for his good advice and help with editing the manuscript.

Appendix A. Supplementary material

Supplementary data to this article can be found online at https://doi.org/10.1016/j.engfracmech.2020.106949.

References

[1] Konieczny A, Henderson T. On formability limitations in stamping involving sheared edge stretching. SAE technical paper 2007-01-0340; 2007.
[2] Mori K, Abe Y, Suzui Y. Improvement of stretch flangeability of ultra high strength steel sheet by smoothing of sheared edge. J Mater Process Tech 2010;210:653–9.
[3] Yoon JI, Jung J, Joo SH, Song TJ, Chin KG, Seo MH, et al. Correlation between fracture toughness and stretch-flangeability of advanced high strength steels. Matter Lett 2016;180:322–6.
[4] Casellas D, Lara A, Frómeta D, Gutiérrez D, Molas S, Pérez Ll, et al. Fracture toughness to understand stretch-flangeability and edge cracking resistance in AHSS. Metall Mat Trans A 2017;48:86–94.
[5] Frómeta D, Tedesco M, Calvo J, Lara A, Molas S, Casellas D. Assessing edge cracking resistance in AHSS automotive parts by the Essential Work of Fracture methodology. J Phys: Conf Ser 2017;896:012102.
[6] Frómeta D, Lara A, Parareda S, Casellas D. Evaluation of edge formability in high strength sheets through a fracture mechanics approach. AIP Conf Proc 2019;2113:160007.
[7] Walp MS. Impact dependent properties of advanced and ultra high strength steel. SAE technical paper 2007-01-0342; 2007.
[8] Larour P, Pauli H, Kurz T, Hebseberger T. Influence of post uniform tensile and bending properties on the crash behaviour of AHSS and press-hardening steel grades. In: Int deep drawing research group (IDDRG) conference; 2010 (Graz, Austria, May 31-June 2 2010).
[9] Larour P, Naito J, Pichler A, Kurz T, Murakami T. Side impact crash behavior of press-hardened steels-correlation with mechanical properties. In: 5th Int conf hot sheet metal forming of high performance steel (CHS2) (Toronto, Canada, May 31- June 3 2015) p. 281–9.

[10] Link TM, Hance BM. Axial and bending crash performance of advanced high-strength steels. In: Int symp on new developments in advanced high-strength steels. Keystone, Colorado, USA; 2017.
[11] Frómeta D, Lara A, Molas S, Casellas D, Rehrl J, Suppan C, et al. On the correlation between fracture toughness and crash resistance of advanced high strength steels. Eng Frac Mech 2019;205:319–32.
[12] Frómeta D, Lara A, Casas B, Casellas D. Fracture toughness measurements to understand local ductility of advanced high strength steels. IOP Conf Ser: Mater Sci Eng 2019;651:012071.
[13] ASTM E1820. Standard test method for measurement of fracture toughness. American Society for Testing and Materials.
[14] ASTM E2472. Standard test method for determination of resistance to stable crack extension under low-constraint conditions. American Society for Testing and Materials.
[15] ISO 22889. Metallic materials — Method of test for the determination of resistance to stable crack extension using specimens of low constraint. International Organization for Standardization.
[16] Cotterell B, Reddel JK. The essential work of plane stress ductile fracture. Int J Fract 1977;267–277.
[17] Mai YW, Pilko KM. The essential work of plane stress ductile fracture of a strain-aged steel. J Mater Sci 1979;14:386–94.
[18] Marchal Y, Delannay F. Comparison of methods for fracture toughness testing of thin low carbon steel plates. Mater Sci Tech 1998;14:1163–8.
[19] Mai YW, Cotterell B. The essential work of fracture for tearing of ductile metals. Int J Fract 1984;24:229–36.
[20] Pardoen T, Hachez F, Marchioni B, Blyth PH, Atkins AG. Mode I fracture of sheet metal. J Mech Phys Solids 2004;52:423–52.
[21] Pardoen T, Marchal Y, Delannay F. Thickness dependence of cracking resistance in thin aluminium plates. J Mech Sol 1999;47:2093–123.
[22] Pardoen T, Marchal Y, Delannay F. Essential work of fracture compared to fracture mechanics—towards a thickness independent plane stress toughness. Eng Fract Mech 2002;69:617–31.
[23] Marchal Y, Walhin JF, Delannay F. Statistical procedure for improving the precision of the measurement of the essential work of fracture of thin sheets. Int J Fract 1997;87:189–99.
[24] Cotterell B, Pardoen T, Atkins AG. Measuring toughness and the cohesive stress–displacement relationship by the essential work of fracture concept. Eng Fract Mech 2005;72:827–48.
[25] Marchal Y, Delannay F. Influence of test parameters on the measurement of the essential work of fracture of zinc sheets. Int J Fract 1996;80:295–310.
[26] Tuba F, Oláh L, Nagy P. The role of ultimate elongation in the determination of valid ligament range of essential work of fracture tests. J Mater Sci 2012;47:2228–33.
[27] Mai YW, Cotterell B. Effects of pre-strain on plane-stress ductile fracture in α -brass. J Mater Sci 1980;13:2296–306.
[28] Wu J, Mai YW. The essential fracture work concept for toughness measurement of ductile polymers. Polym Eng Sci 1996;36:2275–88.
[29] Mai YW, Cotterell B. On the essential work of ductile fracture in polymers. Int J Fract 1986;32:105–25.
[30] Mai YW, Powell P. Essential work of fracture and J-integral measurements for ductile polymers. J Polym Sci 1991;29:785–93.
[31] Martínez AB, Gamez-Perez J, Sanchez-Soto M, Velasco JI, Santana O, Maspoch MLL. The essential work of fracture method- analyzing the post-yielding fracture mechanics of polymers. Eng Fail Anal 2009;16:2604–17.
[32] Lacroix G, Pardoen T, Jacques PJ. The fracture toughness of TRIP-assisted multiphase steels. Acta Mater 2008;56:3900–13.
[33] Wu R, Li J, Li W, Wu XC, Jin X, Zhou S, et al. Effect of metastable austenite on fracture resistance of quenched and partitioned (Q&P) sheet steels. Mater Sci Eng A 2016;657:57–63.
[34] Muñoz R, Lara A, Casellas D. Fracture toughness characterization of advanced high strength steels. In: Int deep drawing research group (IDDRG) conference; 2011 (Bilbao, Spain, June 5-8, 2011).
[35] Gutiérrez D, Ll Pérez, Lara A, Casellas D, Prado JM. Toughness evaluation of high strength steels sheets by means of the essential work of fracture. In: 19th European conference on fracture: fracture mechanics for durability, reliability and safety, ECF 2012; 2012.
[36] Sahoo S, Padmapriya N, Sarathi De P, Chakraborti PC, Ray SK. Ductile tearing resistance indexing of automotive grade DP590 steel sheets: EWF testing using DENT specimens. J Mater Eng Perform 2018;27:2018–23.
[37] Luo ZC, Liu RD, Wang X, Huang MX. The effect of deformation twins on the quasi-cleavage crack propagation in twinning-induced plasticity steels. Acta Mater 2018;150:59–68.
[38] Golling S, Frómeta D, Casellas D, Jonsén P. Influence of microstructure on the fracture toughness of hot stamped boron steel. Mat Sci Eng A 2019;743:529–39.
[39] Kaufman JG, Knoll AH. Kahn-type tear tests and crack toughness of aluminum sheet. Metals Res Stand 1964:151–5.
[40] Garret GG, Knott JF. The influence of compositional and microstructural variations on the mechanism of static fracture in aluminum alloys. Metal Trans A 1978;9:1187–201.
[41] Dumont D, Deschamps A, Brechet Y. On the relationship between microstructure, strength and toughness in AA7050 aluminum alloy. Mat Sci Eng A 2003;356:326–36.
[42] Henn P, Liewald M, Sindel M. Investigation on crashworthiness characterisation of 6xxx series aluminium sheet alloys based on local ductility criteria and edge compression tests. IOP Conf Ser: Mater Sci Eng 2018;418:012125.
[43] Ying L, Lu J, Chang Y, Tang X, Hu P, Zhao K. Optimization evaluation test of strength and toughness parameters for hot-stamped high strength steels. J Iron Steel Res Int 2013;20:51–6.
[44] Lorthios J, Gourgues A F, Cugy P, Scott C. Damage of TWIP steels for automotive application. In: ICF12 Int conference on fracture, Ottawa; 2009.
[45] Faccoli M, Cornacchia G, Gelfi M, Panvini A, Roberti R. Notch ductility of steels for automotive components. Eng Fract Mech 2014;127:181–93.
[46] Rice JR, Paris PC, Merkle JG. Some Further Results of J-Integral Analysis and Estimates. Progress in Flaw Growth and Fracture Toughness Testing. STP 536; 1973. p. 231–45.
[47] Xiong Z, Jacques PJ, Perlade A, Pardoen T. Ductile and intergranular brittle fracture in a two-step quenching and partitioning steel. Scripta Mater 2018;157:6–9.
[48] Xiong Z, Jacques PJ, Perlade A, Pardoen T. Characterization and control of the compromise between tensile properties and fracture toughness in a quenched and partitioned steel. Metall and Mat Trans A 2019.
[49] Rice JR. A path independent integral and the approximate analysis of strain concentration by notches and cracks. J Appl Mech 1968;35:379–86.
[50] Begley JA, Landes JD. The J-integral as a fracture criterion. ASTM STP 514, American Society for Testing and Materials, Philadelphia, PA; 1972. p. 1–20.
[51] Landes JD, Begley JA. The effect of specimen geometry on JIc. ASTM STP 514, American Society for Testing and Materials, Philadelphia, PA; 1972. p. 24–29.
[52] Zhu XK, Leis BN. Revisit of ASTM round robin test data for determining R curves of thin sheet materials. J ASTM Int 2009 [paper ID JAI102510].
[53] ASTM E561. Standard practice for R-curve determination. American Society for Testing and Materials.
[54] Tada H, Paris PC, Irwin GR. The stress analysis of cracks handbook. New York: Third edition. American Society of Mechanical Engineers; 2000.
[55] Hellman D, Schwalbe KH. R-Curve Behaviour of double edge notched tension specimens in plane stress. Mater Sci Eng Technol 1986;17:280–5.
[56] Broberg KB. Crack-growth criteria and non-linear fracture mechanics. J Mech Phys Solids 1971;19:407–18.
[57] Broberg KB. On stable crack growth. J Mech Phys Solids 1975;23:215–37.
[58] Kaufman JG, Hunsicker H. Fracture toughness testing at alcoa research laboratories. Fracture Toughness Test Appl 1965:290–308.
[59] ASTM B871. Standard Test Method for Tear Testing of Aluminum Alloy Products. American Society for Testing and Materials.
[60] Xia L, Shih CF, Hutchinson JW. A computational approach to ductile crack growth under large scale yielding conditions. J Mech Phys Solids 1995;43:389–413.
[61] Zhu XK, Jang SK. J-R curves corrected by load-independent constraint parameter in dcutile crack growth. Eng Frac Mech 2001;68:285–301.
[62] Landes JD, Begley JA. Experimental methods for elastic-plastic and post-yield fracture toughness measurements. Barking, Post-yield fracture mechanics, Applied Science. Publ; 1979.
[63] Akourri O, Louah M, Kifani A, Gilgert G, Pluvinage G. The effect of notch radius on fracture toughness J_{IC}. Eng Frac Mech 2000;65:491–505.
[64] Chaudhari VV, Kulkarni DM, Prakash R. Study of influence of notch root radius on fracture behaviour of extra deep drawn steel sheets. Fatigue Fract Eng Mater Struct 2009;32:975–86.
[65] Mai Y, Cotterell B. Effect of specimen geometry on the essential work of plane stress ductile fracture. Eng Frac Mech 1985;21:123–8.
[66] Cotterell B, Atkins AG. A review of the J and I integrals and their implications for crack growth resistance and toughness in ductile fracture. Int J Fract 1996;81:357–72.
[67] Hance B. Advanced High Strength Steel (AHSS) Performance Levels. SAE Technical Paper 2018-01-0629; 2018.